

Structural and electrical studies on ZnS nanoparticles prepared without using capping agent

HARIT KUMAR SHARMA^a, P. K. SHUKLA^{b*}, S. L. AGRAWAL^{a*}

^aSSI Laboratory, Department of Physics, APS University, Rewa, India

^bI.T.S Engineering College, Greater Noida, India

In this work, zinc sulfide (ZnS) nanoparticles have been synthesized by simple chemical precipitation method without using any capping agent. The synthesized nanoparticles were characterized using XRD, optical microscopy, UV-Vis, FTIR, and impedance spectroscopy. The X-ray diffraction shows that ZnS particles have cubic sphalerite structure with the crystallite size of 10-20 nm. SEM images of nanopowder samples reveal the presence of nanoflakes and agglomerated nanoparticles. Formation of ZnS has been confirmed through the appearance of 714 cm⁻¹ absorption peak. The thermal stability of synthesized nanoparticles has been checked by annealing the material at different temperatures. Transformation of ZnS into ZnO subsequent to annealing has been evidenced from XRD and FTIR studies. UV-Vis spectra exhibited a red shift in the optical absorption on increase in annealing temperature. Variation in electrical conductivity obtained from impedance measurements at different temperatures has been suitably correlated to Davis- Mott model

(Received October 27, 2014; accepted May 7, 2015)

Keywords: Zinc sulfide nanoparticles; II-VI semiconductors; Chemical precipitation method; Optical band gap; Annealing

1. Introduction

Currently there is a great deal of interest in optical and structural properties of nanometer sized semiconductor particles [1]. Additionally, such nanoparticles have exhibited applicability as zero-dimensional quantum confinement material besides application in optoelectronics and photonics [2-3]. Nano semiconductors, including II-VI group semiconductors show significant departures from bulk properties when the scale of confinement approaches to excitonic Bohr radius which sets the length scale for optical process. The photo-emission wavelengths, the band gap and lattice parameter are strongly dependent on the grain size rendering tailorability of these properties as a function of grain size. However, the biggest hurdle in nanotechnology seems to be the control of grain size in a few nanometer range [4-8]. As a consequence, the development of semiconductor nanocrystals of controlled shape and size possessing desired optoelectronic properties has been the subject of intense research. Within the family of nano-semiconductors, Zinc Sulfide has been extensively investigated due to its wide ranging applications in Photoluminescence (PL), Electroluminescence (EL), Cathodoluminescence (CL) devices, Light Emitting Diodes, reflectors and dielectric filters. It has a wide band gap of 3.5-3.8 eV at room temperature and better chemical stability compared to other chalcogenides. Its band can be tuned in the UV region. [9-13].

Annealing treatment is very common in semiconductor processing. It can be used to remove the defects and to test the stability of the crystals at a given temperature under the given ambient conditions, which is important for device purposes. To the best of our

knowledge, there are only few reports on the annealing effects on ZnS [14]. Keeping in view the above, an effort has been made here to study the effect of annealing on the optical, structural and electrical properties of ZnS particles.

2. Experimental

The ZnS nanoparticles have been synthesized by wet chemical co-precipitation method. The analytical grade chemicals zinc chloride (ZnCl₂) and thiourea (NH₂CS-NH₂) (Qualigens chem. India) were used without further purification. Solutions of 0.1M ZnCl₂ and 0.2M NH₂-CS-NH₂ were separately prepared in 100 ml double distilled water. Thiourea solution was then slowly added to zinc chloride solution under continuous stirring. The resulting solution was further stirred for 2 hours and subsequently refluxed in a conical flask at 90 °C for 10 hours. The refluxing temperature was measured by ordinary thermometer. After refluxing, a white 'precipitate' was obtained. The precipitate was then washed with water and ethanol several times and finally dried at 80 °C for 8hours.

The dried samples were annealed in a muffle furnace in air at 200 °C, 400 °C, 600 °C, 800 °C, for 2 hours. XRD studies were conducted on Rigaku make X-ray diffractometer (model Miniflex-II) in 2θ range from 20° to 80° having Cu- α radiation wavelength 1.5406 Å. Optical absorption spectra were recorded with the help of Systronics make UV-VIS Spectrophotometer (model 2203) in 200 nm-1100 nm wavelength range to estimate optical energy gap of the samples. Particle size of ZnS samples was also estimated using optical absorption studies. FTIR spectroscopy of the synthesized samples was

conducted using Thermo Fisher (model iS10) spectrophotometer in the wave number range 4000 cm^{-1} – 400 cm^{-1} . The microstructural details of the samples were investigated using Supra TM 40VP-Field Emission Scanning Electron Microscope, operating at 30 KV. Electrical measurement on ZnS powder pellets were performed by LCR meter (Hioki, model 3520) in the frequency range (40 Hz-100Hz) and temperature range ($30\text{ }^{\circ}\text{C}$ - $70\text{ }^{\circ}\text{C}$).

3. Results

3.1 X-ray diffraction studies

Formation of ZnS powder is apparent from the X-ray diffraction pattern shown in fig1. Existence of diffraction peaks at $2\theta = 28.52^{\circ}$, 33.35° , 48.55° , 56.55° , 59.42° , 70.7° correspond to the presence of sphalerite phase of ZnS in view of JCPDS data. (00-002-0565).

For the sample annealed at $800\text{ }^{\circ}\text{C}$, the peaks appearing at $2\theta = 31.72^{\circ}$, 34.38° , 36.2° , 47.5° , 56.54° , 62.82° , 67.92° , 71.88° in the XRD pattern correspond to wurtzite structure of ZnO (JCPDS Card No. 00-003-0891)

3.2 Optical absorption (UV-Vis absorption) studies

From the optical absorption characteristics of ZnS nanoparticles (fig 2) it is found that the absorption edge due to ZnS nanoparticles lie in the wavelength range of 315–325 nm and it shifts towards larger wavelength side for the sample annealed at temperatures above $400\text{ }^{\circ}\text{C}$. Absorption spectrum show a shift in band gap edges subsequent to annealing of samples which is an indication of the shift of the optical energy band gap. Calculation of the optical band gap shows that it decreases on increasing the annealing temperature with highest value being 3.84 eV for as synthesized ZnS nanoparticles.

3.3 Scanning electron microscopy studies

Higher magnification image of as synthesized ZnS nanopowder (fig. 3a) shows the presence of nanoflakes (10 – 20 nm). When the samples are annealed for two hours at $400\text{ }^{\circ}\text{C}$ these flakes start coalescing to form spherical and rod like shapes of few nanometers due to sufficient thermal energy and which have been reported earlier for ZnO [15]. At such annealing temperatures ZnS starts oxidizing into ZnO due to which necking is observed in SEM image (fig 3b&c).

3.4 FTIR studies

Fig 4 shows the FTIR spectra obtained for as synthesized and heat treated ZnS powder dispersed in KBr pellet. The broad absorption peak appearing at 3450 cm^{-1} is correlated to the O-H stretching vibrations of adsorbed water. The weak peak assignable to either atmospheric CO_2 or S-H absorption shift to lower wave number marginally when the sample is heat treated up to $400\text{ }^{\circ}\text{C}$.

Similarly the band around 1600 cm^{-1} related to –OH bending of water moves towards higher wave number. The absorption peaks observed at 1435 cm^{-1} and 1310 cm^{-1} in as synthesized ZnS sample typically represent C=O vibrations and –OH deformation respectively. The absorption band at 1435 cm^{-1} shifts towards lower wave number (1390 cm^{-1}) subsequent to annealing at $600\text{ }^{\circ}\text{C}$. The presence of –CS-NH amide group is also seen around 1170 cm^{-1} and this too moves to lower wave number upon heat treatment. Careful examination of IR spectra also shows the occurrence of a small band in the wave number range $871\text{--}841\text{ cm}^{-1}$ corresponding to –NH out of plane deformation and CS_2 deformation. The presence of absorption band at 714 and 615 cm^{-1} is noticed which can be related to the formation of ZnS. A peak of ZnO at 415 cm^{-1} is observed in the IR spectra of samples annealed at high temperatures in excess of $400\text{ }^{\circ}\text{C}$.

3.5 Electrical characterization

Fig 5a shows the variation of $\ln\sigma$ as a function of $1000/T$ for all the pre and post heat treated samples. It is noticed that the electrical conductivity drops down on increasing the annealing temperature. The bulk conductivity of as synthesized and heat treated ZnS particles show two distinct stages of conductivity variation with temperature separated by non linear region. This observation suggests two transport mechanisms described by separate activation energies.

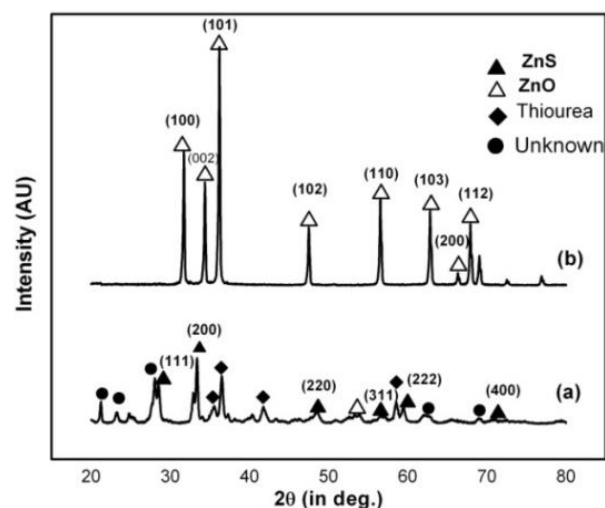


Fig. 1: XRD pattern of as (a) synthesized ZnS powder and (b) subsequent to annealing at $800\text{ }^{\circ}\text{C}$.

4. Discussion

4.1 X-ray Diffraction studies

Fig 1 depicts the XRD pattern for as synthesized and annealed ($800\text{ }^{\circ}\text{C}$) ZnS powder. The nanocrystalline nature of as synthesized ZnS powder is apparent from the X-ray diffraction pattern (fig 1a). The observed diffraction peaks

match very well in terms of relative intensity and peak positions with JCPDS data file for ZnS (00-002-0565). Moreover, few additional unknown peaks also appear which correspond to either the presence of thiourea and /or thiourea zinc chloride complex formed during the synthesis. For the sample annealed at 800 °C, the peaks appearing in the XRD pattern (fig 1b) correspond to wurtzite structure of ZnO (JCPDS data 00-003-0891). The average crystallite size has been calculated using the well known Debye-Scherrer relation [16].

$$D = \frac{k\lambda}{\beta_{hkl} \cos \theta} \quad (1)$$

where D = average crystallite size, k = shape factor (0.9), λ = the wavelength of incident X-ray beam (1.5406 Å), θ = the angle of the diffraction peak and β_{hkl} is the full width at half maximum (FWHM) of the XRD peak appearing at the diffraction angle θ . The average calculated crystallite size of as synthesized and annealed samples is found to vary between 13-35 nm (table 1). Also it is found to increase with increase in annealing temperature.

Table.1: Particle size and optical band gap data for as synthesized and annealed ZnS samples obtained from XRD and UV-Vis experiments

Particulars of ZnS Sample	Crystallite Size (XRD analysis) nm	Optical Band gap eV	Particle Size (UV-Vis analysis) nm
As-synthesized	12.9	3.84	6.44
Annealed at 400 °C for 2 hrs	-	3.83	6.91
Annealed at 600 °C for 2 hrs	-	3.66	5.88*
Annealed at 800 °C for 2 hrs	35.5	3.58	6.87*

* Calculated using E_g (bulk) for ZnO

These results ascertain nanocrystalline behavior of synthesized ZnS powder which transform into ZnO nanoparticles on annealing at higher temperature (> 400 °C) under ambient conditions.

4.2 Optical Absorption (UV-Vis Absorption) studies

As said earlier optical absorption spectrum recorded for both unannealed and annealed samples indicate a shift in optical energy band gap of synthesized nano particles.

The transmittance (T) at different wavelength (λ) was measured in the spectra and then absorption coefficient (α) was calculated using the well known Beer-Lambert's relation

$$\alpha = 2.303.A/t \quad (2)$$

The absorption coefficients (α) and the incident photon energy (hv) are interrelated by the well known Tauc equation [17]

$$(\alpha hv)^2 = A (hv - E_g)^n \quad (3)$$

where E_g is the band gap of the material, A a constant and exponent n depends on the type of transition. For direct allowed transition $n=1/2$, while it is 2 and 3/2 for indirect allowed, and direct forbidden transition respectively. Considering direct allowed transition for ZnS a graph of $(\alpha hv)^2$ versus hv was plotted (fig 2) to estimate the band gap from the extrapolation of straight line to hv -axis [i.e., where $(\alpha hv)^2 = 0$]. Table 1 lists the so obtained optical energy gap for as synthesized and as well as annealed samples which are similar to the earlier reported values. It is apparent that the optical band gap decreases with increasing annealing temperature with highest value 3.84 eV for as synthesized ZnS nanoparticles. This red shift of band gap takes place essentially due to the growth of grain size and decrease in defect states near the band edges. The change in band gap changes can be correlated to the size of nanoparticles using the effective mass model which is used to study the size dependent optical properties of quantum dots (QD) system. According to this model [17-19]

$$E_{g(nano)} = E_{g(bulk)} + \frac{h^2}{8R^2} \left(\frac{1}{m_h^*} + \frac{1}{m_e^*} \right) - \frac{1.8e^2}{4\pi R \epsilon_r \epsilon_0} \quad (4)$$

where h is the Planck's constant, R the radius of nanoparticles, ϵ_r the dielectric constant of the material, and m_e^*, m_h^* are the effective mass of electron and hole. The second term involves the confinement effect while the third term results from coulomb interaction. The effect of third term is extremely small in case of nanoparticles and hence neglected for calculations. The particle size calculated using above model is also listed in table 1 along with the particle size extracted from XRD measurements. These values confirm the nanometric dimension of ZnS particles synthesized in the present investigation.

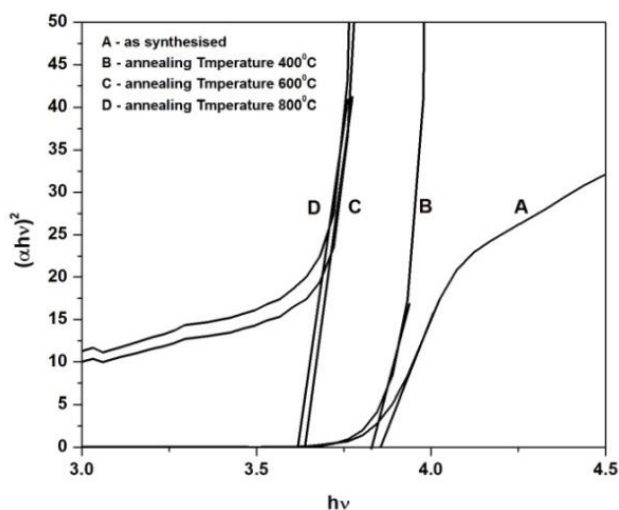


Fig. 2: Variation of $(\alpha hv)^2$ against photon energy (Tauc's plot) for the determination of optical band gap of ZnS nanoparticles

4.3 SEM Studies

Fig 3 shows SEM images of as synthesized and annealed sample of ZnS nanopowder. Presence of flake type structure with nano dimensions (10-20nm) in higher magnification image of the as synthesized ZnS powder (fig. 3a) reveal the formation of nanosized ZnS powder. After annealing at higher temperature (above 400 °C) necking of flakes starts due to oxidation of ZnS to ZnO (fig 3b&c). Thus, annealing of samples results in the phase change from ZnS to ZnO and the formation of larger agglomerates. Essentially, due to oxidation of ZnS, rock like structures of ZnO are formed which contains porous rods of the size of a few microns (fig 3d). Interestingly the low magnification image [fig 3b] depicts the occurrence of nanotube type structure which has not been reported earlier for ZnS samples. This could be possibly due to the presence of a catalyst which is generally required to obtain nanotubes.

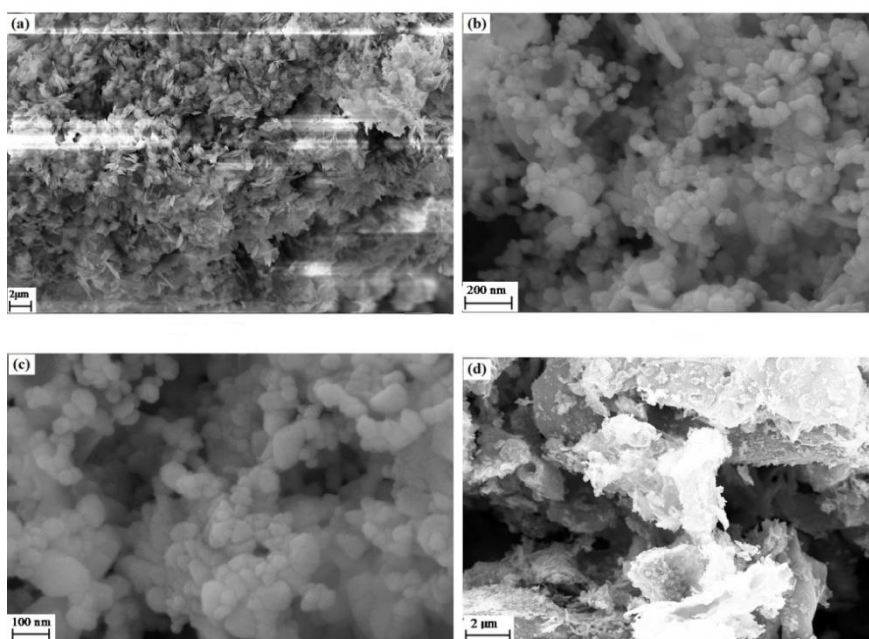
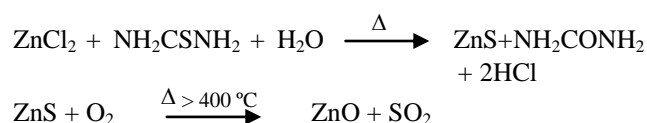


Fig 3: SEM images of ZnS samples (a) as-synthesized, (b & c) annealed at 400 °C and (d) annealed at 800 °C.

4.4 FTIR Studies

The presence of absorption peaks around 1170 cm^{-1} , 977 cm^{-1} corresponding to -CS-NH amide group and N-H deformation shows the presence of unreacted thiourea. Also the occurrence of a small band in the IR spectra of fig 4 in the wave number range $871\text{--}841\text{ cm}^{-1}$ corresponds to -NH out of plane deformation and CS_2 deformation which reaffirms the presence of thiourea during synthesis of ZnS powder. This band is seen to converge and shift to the higher wave number side upon heat treatment. The presence of absorption band at 714 cm^{-1} confirms the formation of ZnS [15]. Formation of ZnS nanoparticles is further evidenced through the presence of absorption

vibration at 615 cm^{-1} . The appearance of new peak at 415 cm^{-1} in the IR spectrum of ZnS powder annealed at higher temperatures ($>400\text{ }^\circ\text{C}$), may be attributed to the transformation of ZnS to ZnO at such temperatures [20-22]. Thus, following reactions seems to validate these observations.



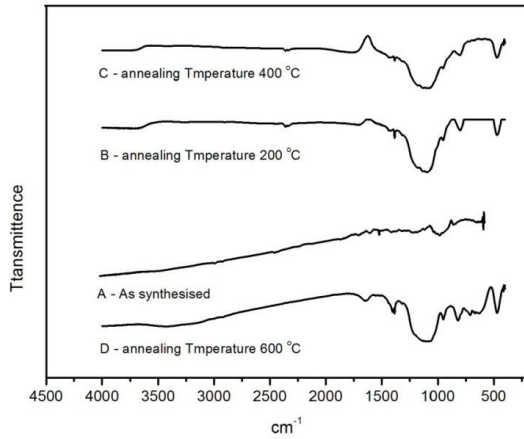


Fig. 4: FTIR Spectra of as synthesized and annealed ZnS samples

4.5 Electrical Characterization

The drop in conductivity (fig 5a) with an increase in annealing temperature can be associated to decrease in defect states and which in turn increases the energy band gap of ZnS particles [23]. Further, observed bulk conductivity behavior ZnS particles suggests two transport mechanisms described by separate activation energies. Such a behavior is typical of amorphous semiconductors and best described by well known Davis Mott model [24, 25]. According to this model, the standard energy band scheme describing a crystalline material changes in the amorphous case so that the valence and the conduction bands stretch out and develop a tail while a middle allowed band (compensated levels) also goes up near the center of the forbidden band gap. Carriers possessing energies within the tails and the central band are described by localized states while for other energies, the carriers lie in the extended states. In the Davis – Mott model, there are three mechanisms of charge transport with each dominating in different temperature ranges:

(i) At the highest temperatures, the carriers are excited into extended states where they acquire mobilities orders of magnitude greater than in the localized states;

(ii) At the medium temperatures, the carriers are excited into localized states in the valance and conduction band tails; and

(iii) At low temperatures, conduction occurs by tunneling between states located in the central band near the Fermi level (variable range hopping).

In case (i) the temperature dependence of conductivity $\sigma_{DC}(T)$ exhibits Arrhenius behavior with activation energy that is equal to the difference between the Fermi level and the energy that defines the boundary between localized and extended states; In case (ii), electrical conduction occurs by thermally activated hopping and $\sigma_{DC}(T)$ still follows Arrhenius behavior but with different activation energy involving Fermi level energy, the energies of tail edges, and hopping activation energy and here pre-exponential factor acquires weak temperature dependence.

Finally for case (iii), conduction is the range phonon-assisted tunneling also known as “variable-range hopping” and in this case $\sigma_{DC}(T)$ can be expressed as

$$\sigma_{DC(T)} = \frac{\sigma_0}{\sqrt{T}} \exp \left[- \left(\frac{T_0}{T} \right)^{1/4} \right] \quad (5)$$

where σ_0 and T_0 are parameters of Davis-Mott model [24-25].

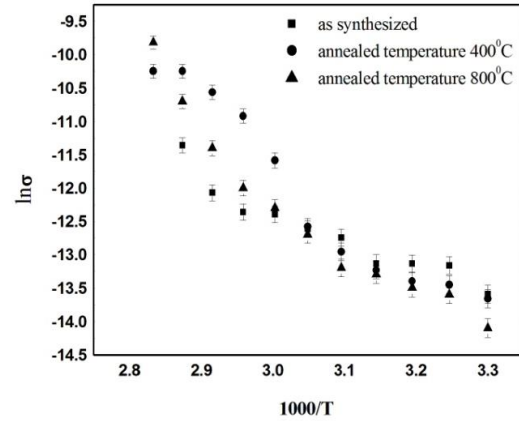


Fig. 5a: Variation of DC electrical conductivity with temperature of as synthesized and annealed ZnS samples

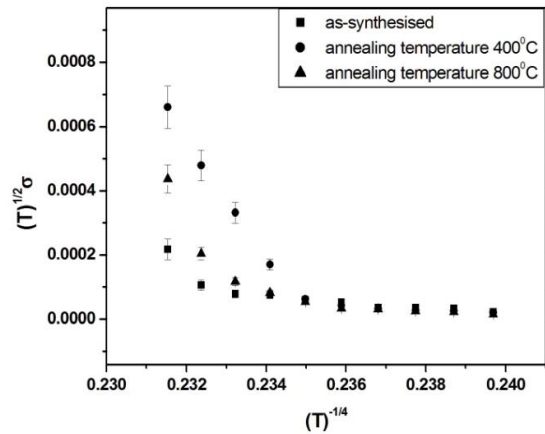


Fig. 5b: DC conductivity data fit with to Mott-Davis model for as-synthesized and annealed ZnS samples

Table 2: Estimated Mott parameter for ZnS samples

Particulars of ZnS Sample	$\sigma_0(\text{K}^{1/2} \text{ S cm}^{-1})$	$T_0(^{\circ}\text{K})$
As-synthesized	6.05×10^{19}	3.0×10^9
Annealed at 400 °C for 2hrs	4.1×10^{42}	4.3×10^{10}
Annealed at 800 °C for 2hrs	5.2×10^{40}	3.7×10^{10}

The Activation energy corresponding to first case suggest the existence of high density of localized states while the second case represents carrier transport across grain boundaries by thermal excitation. The information about $\sigma_{DC}(T)$ extracted from the observed conductivity data for ZnS has been analyzed in view of the above said three mechanisms (i) - (iii) of the Davis-Mott model. Our analysis indicates that the conductivity data is best described by mechanism (iii) as can be seen in fig 5b where a fit to the behavior represented by Eq. (5) is reasonably good for temperature in the range 300 - 360 °K. Mott parameters σ_0 & T_0 were extracted from the best fit line and tabulated in table 2 for all the samples.

5. Conclusions

Structural, optical and electrical properties of ZnS nanoparticles obtained using chemical co-precipitation method have been studied for as synthesized as well as annealed samples. XRD measurements of as synthesized samples reveal the formation of ZnS nanoparticles of size 10-30 nm possessing sphalerite phase. The ZnS powder completely transformed into wurtzite ZnO phase after annealing at 800 °C. Existence of 714 cm^{-1} peak in FTIR spectra ascertain the formation of ZnS nanoparticles. The formation of ZnS nanoflakes is seen in the SEM examination which converts into globular and rod shaped structure subsequent to annealing. UV-Vis spectra shows shifting of optical band gap value towards lower side after annealing. The enhancement in the conductivity subsequent to annealing at higher temperature is related to transformation of ZnS to ZnO phase. Overall conductivity response is found to be best described by Mott-Davis model.

Acknowledgments

The authors are thankful to Ajay Dhar, and D.K Mishra of Materials Physics & Engineering Division, CSIR-National Physics Laboratory, New Delhi, India for stimulating discussion and for providing technical support to perform X-ray diffraction and Scanning Electron Microscopy of the samples.

References

- [1] A. Jaeger-waday, Sol. Energy **77**, 667 (2004)
- [2] R. R. Prabhu, M. Abdul Khadar, Pramana **5**, 801 (2005)
- [3] X. Fang, Y. Bando, U. K. Gautam, T. Zahi, H. Zeng, X. Xu, M. Lio, D. Golberg, Critical Reviews in Solid State and Materials Sciences **34**, 90 (2009)
- [4] K. Rajeswar, N. R. Tacconi, C. R. Chenthamarakshan, Chem. Mater. **13**, 2765 (2001)

- [5] A. P. Alivisatos, Science **271**, 933 (1996)
- [6] M. A. Gorer, S Anderson, R. M. Penner, J. Chem. Phys. B **101**, 5895 (1997)
- [7] G. Henshaw, I. P. Parkin, G Shaw Chem. Commun. **10**, 1095 (1996)
- [8] T. Hirai, Y. Bando, I. Komasaawa, J. Chem. Phys. B **106**, 8967 (2002)
- [9] Xiaosheng Fang, Tianyou Zhai, Ujjal K. Gautam, Liang Li, Limin Wua, Yoshio Bando, Dmitri Golberg, Progress in Materials Science **56**, 175 (2011)
- [10] N. Chestnoy, R. Hull, L. E. Brus, J. Chem. Phys. **85**, 2237 (1996)
- [11] C. S. Hwang, I. H. Cho, Bull. Korean Chem. Soc. **26**, 1776 (2005)
- [12] L. E. Brus, J. Chem. Phys. **80**, 4403 (1984)
- [13] A. I. Cadis, A. R. Tomsa, M. Stefan, R. Grecu, L. Barbu- Tudoran, L. Silagi- Dumitrescu, E. J. Popovici, J. Optoelectron. Adv. Mater. **12**(1), 111 (2010)
- [14] G. Murali, D. Amarnatha Reddy, B. Poornaprakash, R. P. Vijaylakshmi, N. Madhusudhana Rao, Optoelectron. Adv. Mater. – Rapid Commun **5**(9) 928 (2011)
- [15] X. Zou, E. Ying and S. Dong, Nanotechnology **17**, 4758 (2006)
- [16] T. Khalid Al-Rasoul, K. Nada Abbas, J. Zainb Shanana, Int. J. Electrochem. Sci. **8**, 5594 (2013)
- [17] C. M. Liu, X.T. Zu, Q. M. Wei, L. M. Wang J. Phys. D, Appl. Phys. **39**, 2494 (2006)
- [18] D. C. Onwudiwe and P. A. Ajibade, Int. J. Mol. Sci. **12**, 5538 (2011)
- [19] T. Khalid Al-Rasoul, K. Nada Abbas, J. Zainb Shanana, Int. J. Electrochem. Sci., **8**, 5594 (2013)
- [20] R. Wahab, S. G. Ansari, Y. S. Kim, M. S. Dhage, H. K. Seo, M. Song, H. S. Shin, Met. Mater. Int. **15**, 453 (2009)
- [21] N. Goswami, P. Sen, Solid State Comm. **132**, 791(2004)
- [22] X. Zou, E. Ying, S. Dong, Nanotechnology, **17**, 4758 (2006)
- [23] A. U. Ubale, D. K. Kulkarni, Bull. Mater. Sci. **28**, 43 (2005)
- [24] P. Nagels, M. H. Brodsky (Ed), Topics in Applied Physics, Amorphous Semiconductors, Springer-Verlag, (1979)
- [25] N. F. Mott and E. A. Davis, Electronic Processes in Non-Crystalline Materials, Clarendon, Oxford Univ. Press (1979)

*Corresponding author: sla_ssi1956@rediffmail.com & pks.vits@gmail.com